INTERNATIONAL JOURNAL FOR NUMERICAL METHODS IN FLUIDS
Int. J. Numer. Meth. Fluids 2001; **37**: 65–86 (DOI: 10.1002/fld.165)

Numerical solution of Navier–Stokes equations using multiquadric radial basis function networks

Nam Mai-Duy and Thanh Tran-Cong*,[1]

Faculty of Engineering and Surveying, University of Southern Queensland, Toowoomba, Queensland, Australia

SUMMARY

A numerical method based on radial basis function networks (RBFNs) for solving steady incompressible viscous flow problems (including Boussinesq materials) is presented in this paper. The method uses a 'universal approximator' based on neural network methodology to represent the solutions. The method is easy to implement and does not require any kind of 'finite element-type' discretization of the domain and its boundary. Instead, two sets of random points distributed throughout the domain and on the boundary are required. The first set defines the centres of the RBFNs and the second defines the collocation points. The two sets of points can be different; however, experience shows that if the two sets are the same better results are obtained. In this work the two sets are identical and hence commonly referred to as the set of centres. Planar Poiseuille, driven cavity and natural convection flows are simulated to verify the method. The numerical solutions obtained using only relatively low densities of centres are in good agreement with analytical and benchmark solutions available in the literature. With uniformly distributed centres, the method achieves Reynolds number $Re = 100\,000$ for the Poiseuille flow (assuming that laminar flow can be maintained) using the density of 11×11, $Re = 400$ for the driven cavity flow with a density of 33×33 and Rayleigh number $Ra = 1\,000\,000$ for the natural convection flow with a density of 27×27. Copyright © 2001 John Wiley & Sons, Ltd.

KEY WORDS: mesh-free method; Navier–Stokes equations; radial basis function networks; streamfunction–vorticity formulation

1. INTRODUCTION

Continuum mechanics problems often lead to a set of partial differential equations (PDEs) together with a set of boundary conditions. The finite difference method (FDM) (cf. Roache [1], Smith [2]), the finite element method (FEM) (cf. Cook *et al.* [3], Fletcher [4], Hughes [5], Reddy and Gartling [6], Zienkiewicz and Taylor [7]) and the finite volume method (FVM)

* Correspondence to: Faculty of Engineering and Surveying, University of Southern Queensland, Toowoomba, Queensland 4350, Australia. Tel.: + 61 7 46312539; fax: + 61 7 46312526.
[1] E-mail: trancong@usq.edu.au

Received March 2000
Revised August 2000

(cf. Patankar [8]) are well established numerical methods to solve these equations. As the name suggests, these methods rely on the discretization of the domain of analysis into a number of 'finite elements' (FEs) which are of standard 'shape', i.e. they are defined by a certain fixed topology in terms of a number of nodes. The task of breaking the original domain of analysis into a set of FEs is non-trivial due to the rigid structure required by this methodology. This difficulty is particularly acute in three-dimensional problems or even in two-dimensional problems with moving boundaries, free surfaces or complex boundaries. It is possible to devise an alternative element-free method based on neural network methodology. Radial basis function networks (RBFNs) have become one of the main fields of research in numerical analysis (cf. Powell [9], Broomhead and Lowe [10], Poggio and Girosi [11], Haykin [12]). Interest in RBFNs (especially ones based on multiquadric radial basis functions or MQRBF) as numerical methods for solving PDEs has been increasing recently. The RBFN-based methods require only a set of unstructured discrete collocation points to 'discretize' the governing equations, which naturally offers the advantage of being mesh-free. Essentially, in a typical RBFN-based method each of the relevant variables, such as u, is approximated in terms of weighted RBFs (or neurons) which incorporate two adjustable parameters, namely the centres and the widths, as follows:

$$u(\boldsymbol{x}) = \sum_{i=1}^{m} w^{(i)} g^{(i)}(\boldsymbol{x})$$

where $\{w^{(i)}\}_{i=1}^{m}$ is the set of weights; $\{g^{(i)}\}_{i=1}^{m}$ is the set of radial basis functions and m is the number of centres. The basis functions contain the centre and width parameters. In the case of self-organized networks, the centres and the widths are chosen in advance and hence the set of original unknowns in the governing equations can be transformed into a set of unknown weights of the RBFNs, which is to be found. When the RBFN representations of the variables are substituted in the governing equations, which are collocated at random collocation points as shown in Figure 1, a set of algebraic equations in terms of the RBFN weights is obtained. The system matrix may or may not be square depending on particular formulations. The present method generally results in a non-square system which is solved by a method based on the general linear least square principles. It is important to note that the accuracy of the RBFN solution is influenced by a parameter that is usually referred to as the width of basis function. The value of this parameter controls the shape of the basis function or the response of the associated neuron. Large or small values make the neuronal response too flat or too peaked respectively, and therefore both of these two extreme conditions should be avoided. By numerical experimentation, Kansa [13] found that the best results achieved by multiquadric approximation scheme occurred when the shape (width) parameter a^2 is varied according to the following expansion:

$$a^{(i)2} = a^2_{\min}(a^2_{\max}/a^2_{\min})^{(i-1)/(m-1)} \tag{1}$$

where $a^2_{\max}$ and $a^2_{\min}$ are input parameters, $1.0e1 \leq (a^2_{\max}/a^2_{\min}) \leq 1.0e6$ (Moridis and Kansa [14]); superscript (i) indexes the ith centre and m is the number of centres. Based on formula (1), Kansa [15], Dubal [16] and Sharan *et al.* [17] have applied the multiquadric approximation

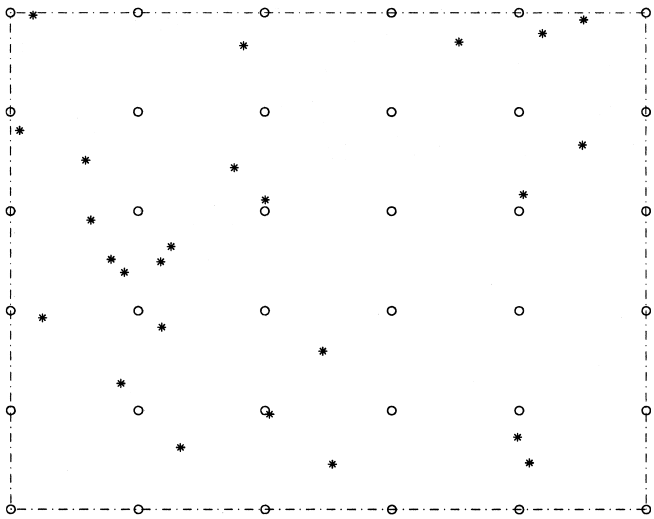

Figure 1. RBF centres and collocation points. Legends: ○, RBF centre; *, collocation point. RBF centres are regularly distributed for best results while collocation points can be random [18].

scheme successfully for the numerical solution of PDEs (Poisson equations). Recently, Mai-Duy and Tran-Cong [18,19] have developed new methods based on RBFNs for approximating functions and demonstrated the capabilities of the methods with a solution of Poisson equations. The so-called direct RBFN (DRBFN) and indirect RBFN (IRBFN) methods were studied and it was found that the IRBFN method yields excellent results. In contrast to the approach taken by other authors as reviewed above, in the present methods the width of the ith neuron (centre) $a^{(i)}$ is determined according to the following simple relation (Moody and Darken [20]):

$$a^{(i)} = \beta d^{(i)} \tag{2}$$

where β is a factor, $\beta > 0$ and $d^{(i)}$ is the distance from the ith centre to the nearest neighbouring centre. Relation (2) indicates that it is reasonable to assign a larger width where the centres are widely separated from each other and a smaller width where the centres are closer. The results obtained [18,19] show that the IRBFN method achieves a better accuracy than the DRBFN method over a wide range of β. The practical choice of RBF width $a^{(i)}$ is much simpler with both of the above methods. In this paper the IRBFN method is further developed to obtain numerical solutions of the Navier–Stokes equations. The system of differential equations may be in terms of velocity and pressure, velocity and vorticity or stream function and vorticity. However, for two-dimensional problems, numerical methods usually employ the streamfunction–vorticity formulation rather than the velocity–pressure formulation. The advantage of the streamfunction–vorticity formulation over

the velocity–pressure formulation is that the number of variables is reduced to two and the continuity equation is automatically satisfied. The streamfunction–vorticity formulation for two-dimensional problems is considered here because of the lesser number of unknowns involved and the principle of the proposed method is applicable to other formulations for two- and three-dimensional problems. The paper is organized as follows. Firstly, the IRBFN method is presented for steady viscous flows in Section 2 and then for natural convection (Boussinesq approximation) flows in Section 3. Numerical examples of planar Poiseuille, driven cavity and natural convection flows in a square slot are reported to illustrate the present method. Finally, some concluding remarks are given in Section 4.

2. INCOMPRESSIBLE VISCOUS FLOW PROBLEMS

2.1. Governing equations

The Navier–Stokes equations for steady incompressible planar viscous flows, subject to negligible body forces, are expressible in terms of the streamfunction ψ and the vorticity ω as follows:

$$\omega + (\psi_{,11} + \psi_{,22}) = 0, \quad \mathbf{x} \in \Omega \tag{3}$$

$$v(\omega_{,11} + \omega_{,22}) = \psi_{,2}\omega_{,1} - \psi_{,1}\omega_{,2}, \quad \mathbf{x} \in \Omega \tag{4}$$

where v is the kinematic viscosity; $\mathbf{x}$ is the position vector of a point in the analysis domain Ω; $\psi_{,i} \equiv \partial\psi/\partial x_i$; $\psi_{,ij} \equiv \partial^2\psi/\partial x_i\,\partial x_j$ and similarly for the partial derivatives of ω.

The vorticity and streamfunction are defined by

$$\omega = u_{2,1} - u_{1,2}, \quad \mathbf{x} \in \Omega \tag{5}$$

$$\psi_{,2} = u_1, \qquad \psi_{,1} = -u_2, \quad \mathbf{x} \in \Omega \tag{6}$$

where u_1 and u_2 are the components of the velocity vector and $u_{i,j} \equiv \partial u_i/\partial x_j$.

Let L be a characteristic length and U a characteristic speed of the flow, the variables are non-dimensionlized as follows:

$$u_i' = \frac{u_i}{U}, \qquad x_i' = \frac{x_i}{L}, \qquad \omega' = \frac{\omega}{U/L} \quad \text{and} \quad \psi' = \frac{\psi}{UL} \tag{7}$$

From here on, the primes are dropped for brevity. The dimensionless governing equations are

$$\omega + (\psi_{,11} + \psi_{,22}) = 0, \quad \mathbf{x} \in \Omega \tag{8}$$

$$\omega_{,11} + \omega_{,22} = Re(\psi_{,2}\omega_{,1} - \psi_{,1}\omega_{,2}), \quad \mathbf{x} \in \Omega \tag{9}$$

where $Re = UL/v$ is the Reynolds number. The streamfunction equation (8) is known as the kinematic condition since it is simply the property of the flow field and does not depend on what causes the flow. The vorticity transport equation (9) is known as the kinetic condition since it is derived from the kinetics of motion; in this case, Newton's second law and the linear constitution equations. In the present method, the equations for ω and ψ together with boundary conditions are solved simultaneously to obtain the solution.

2.2. Boundary conditions

The general boundary conditions on the ψ are expressed in terms of the velocity as

$$\psi_{,1} = -u_{20}, \quad \psi_{,2} = u_{10}, \quad \mathbf{x} \in \Gamma \tag{10}$$

where Γ is the boundary of the analysis domain Ω. On a non-porous wall, no-slip boundary condition yields Dirichlet and Neumann boundary data as follows

$$\psi = 0, \quad \psi_{,n} = v_{\mathrm{W}}, \quad \mathbf{x} \in \Gamma \tag{11}$$

where v_{W} is the tangential wall velocity and n is the local direction normal to the wall.

Equations (8)–(11) are a complete specification of the problem to be solved.

2.3. Numerical formulation based on RBFNs

The basic derivation of the present RBFN method is given elsewhere [18,19]. Specifically, in the present IRBFN highest-order derivatives are expressed in terms of RBFN first, followed by successive symbolic integrations to obtain closed form expressions for lower-order derivatives and finally the function(s) itself. For example

$$\psi_{,ii}(\boldsymbol{x}) = \sum_{i=1}^{m} w^{(i)} g^{(i)}(\boldsymbol{x})$$

$$\psi_{,i}(\boldsymbol{x}) = \int \psi_{,ii}(\boldsymbol{x})\, \mathrm{d}x_i$$

$$\psi^{i}(\boldsymbol{x}) = \int \psi_{,i}(\boldsymbol{x})\, \mathrm{d}x_i$$

The closed form representations thus obtained are then substituted into the governing equations and boundary conditions to 'discretize' the system via the mechanism of point collocation [18]. The application of the method to the present problem, e.g. Equations (8) and (9) with boundary conditions (10), results in the following sum-squared error (SSE), which is to be minimized in the sense of the general linear least square principle

$$\begin{aligned}\mathrm{SSE} = & \sum_{\boldsymbol{x}^{(i)}\in\Omega} (\psi_{,11}(\boldsymbol{x}^{(i)}) + \psi_{,22}(\boldsymbol{x}^{(i)})) + \omega^1(\boldsymbol{x}^{(i)})]^2 + \sum_{\boldsymbol{x}^{(i)}\in\Omega} (\omega_{,11}(\boldsymbol{x}^{(i)}) + \omega_{,22}(\boldsymbol{x}^{(i)})) \\ & - Re[\psi_{,2}(\boldsymbol{x}^{(i)})\omega_{,1}(\boldsymbol{x}^{(i)}) - \psi_{,1}(\boldsymbol{x}^{(i)})\omega_{,12}(\boldsymbol{x}^{(i)})]\}^2 \\ & + \sum_{\boldsymbol{x}^{(i)}\in\Omega} [(\psi^1(\boldsymbol{x}^{(i)}) + \psi^2(\boldsymbol{x}^{(i)})]^2 + [\omega^1(\boldsymbol{x}^{(i)}) - \omega^2(\boldsymbol{x}^{(i)})]^2\} \\ & + \sum_{\boldsymbol{x}^{(i)}\in\Omega} [(\psi_{,1}(\boldsymbol{x}^{(i)}) + u_{2o}(\boldsymbol{x}^{(i)})]^2 + [\psi_{,2}(\boldsymbol{x}^{(i)}) - u_{1o}(\boldsymbol{x}^{(i)})]^2\} \end{aligned} \tag{12}$$

where $\boldsymbol{x}^{(i)}$ is the ith collocation point, $i = [1, n]$ and n is the number of collocation points. In the present problem some non-linear terms appear, i.e. $\psi_{,2}\omega_{,1}$ and $\psi_{,1}\omega_{,2}$, which require a different numerical treatment. In general, the non-linear terms are estimated based on some current approximate values of the variables leading to an iterative procedure which is as follows:

1. Guess the initial velocity and vorticity fields for the first iteration (usually initialized to zero in the present work);
2. Compute the non-linear terms (the convection term) using the current estimate of the velocity and vorticity fields

$$\psi_{,2}(\boldsymbol{x}^{(i)})\omega_{,1}(\boldsymbol{x}^{(i)}) - \psi_{,1}(\boldsymbol{x}^{(i)})\omega_{,2}(\boldsymbol{x}^{(i)}),\ i = [1, n]$$

3. Solve (12) in the sense of the general linear least square principle for the new estimate of the velocity and vorticity fields;
4. Check for convergence. Convergence measure (CM) at the kth iteration is defined as follows:

$$\mathrm{CM} = \sqrt{\frac{\sum_{i=1}^{n} (\omega^k(\boldsymbol{x}^{(i)}) - \omega^{k-1}(\boldsymbol{x}^{(i)}))^2}{\sum_{i=1}^{n} (\omega^k(\boldsymbol{x}^{(i)}))^2}} \tag{13}$$

   The solution procedure is terminated when $\mathrm{CM} < \mathrm{tol}$, where tol is a set tolerance;
5. If not yet converged, repeat from step 2;
6. If converged, stop.

Apart from the mesh-free property, another powerful feature of the present method is its flexibility in the incorporation of extra boundary conditions. This is possible owing to the general least square principle underlining the present formulation which allows non-square system matrix. Furthermore, the algorithm presented above indicates that the non-linear terms are estimated using the value of field variables obtained in the previous iteration and thus the singular value decomposition of the system matrix needs to be done only once for all values of Reynolds number and also for all subsequent iterations, provided that the centre distribution, the collocation point distribution and β are fixed, which is the case in the present method.

2.4. Numerical examples

To investigate the abilities of the numerical method, two incompressible viscous flow problems are simulated and the results obtained are presented in this section. All the numerical solutions here for each Reynolds number are obtained starting from the condition of fluid at rest. In all following examples, the set of collocation points chosen is also the set of RBF centres ($n = m$). The tolerance for convergence criterion is set at $\mathrm{tol} = 1.0e - 4$. A noteworthy feature of the present work is that excellent results are obtained with the use of only uniformly distributed collocation points at relatively low density in contrast with higher density and/or graded meshes used by other methods reported in the literature.

2.4.1. A simple test problem—Poiseuille flow in a channel. A laminar flow between two parallel plates is assumed to exist in the x_1 direction and to be solved in a domain: $0 \le x_1 \le 1$, $-1 \le x_2 \le 1$ with the boundary conditions

$$u_1 = u_0(1 - x_2^2), \quad u_2 = 0 \quad \text{on the lines } x_1 = 0 \text{ and } x_1 = 1 \tag{14}$$

$$u_1 = 0, \quad u_2 = 0 \quad \text{on the lines } x_2 = -1 \text{ and } x_2 = 1 \tag{15}$$

where u_0 is the maximum velocity in the channel (Figure 2). In this case, the Reynolds numbers, with $U = u_0$ and $L = 2$, associated with the flow becomes $Re = 2u_0/v$. Owing to symmetry, only half of the fluid domain is considered and thus the boundary conditions used in the streamfunction–vorticity formulation are

$$\psi_{,1} = 0, \quad \psi_{,22} = 0 \quad \text{on the line } x_2 = 0 \tag{16}$$

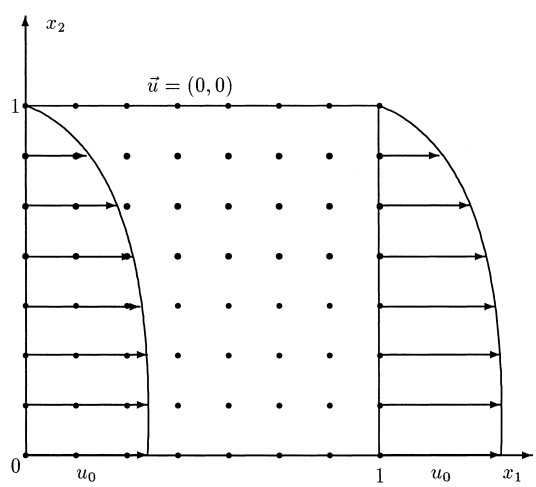

Figure 2. Poiseuille flow: note that the centre distribution is schematic only.

$$\psi_{,1} = 0, \quad \psi_{,2} = u_0(1 - x_2^2) \quad \text{on the lines } x_1 = 0 \text{ and } x_1 = 1 \tag{17}$$

$$\psi = 0, \quad \psi_{,2} = 0 \quad \text{on the line } x_2 = 1 \tag{18}$$

The steady solution is known analytically which is given by

$$u_{1e} = u_0(1 - x_2^2), \qquad u_{2e} = 0 \tag{19}$$

Here the fluid flow inside the computational domain needs to be estimated numerically by the present method. As mentioned above, the RBFN solution depends on the value of RBF width β. Two studies of the parameter β are carried out using a uniform centre density of 11×11. The first is to investigate the effect of β on the quality of the solution at $Re = 100$. The value of β is taken from 5.0 to 10.0 with an increment of 1.0. The method is convergent for all values of β with a high accuracy as shown in Table I where the error norm N_e used here is the norm of the error of the velocity field

$$N_e = \sqrt{\frac{\sum_{i=1}^{n} [(u_1(\boldsymbol{x}^{(i)}) - u_{1e}(\boldsymbol{x}^{(i)}))^2 + (u_2(\boldsymbol{x}^{(i)}) - u_{2e}(\boldsymbol{x}^{(i)}))^2]}{\sum_{i=1}^{n} [(u_{1e}(\boldsymbol{x}^{(i)}))^2 + (u_{2e}(\boldsymbol{x}^{(i)}))^2]}} \tag{20}$$

The second study is to investigate the convergence radius of Reynolds number. Table II shows that Re up to 100 000 can be easily achieved with $\beta = 8.0$ (assuming that laminar flow can be maintained). The velocity profile corresponding to this high Reynolds number was found to be in excellent agreement with the analytical solution.

2.4.2. A benchmark problem—driven cavity flow. We turn our attention now to solve the standard benchmark problem of a lid-driven unitary square cavity (Roache [21], Ghia *et al.* [22]) whose top wall moves with a uniform velocity of 1.0 in its own plane as a model problem for checking and evaluating the numerical method (Figure 3). Here the Reynolds number $Re = UL/v = 1/v$. Applying (11) to the present problem, the boundary conditions imply

Table I. Effect of β on the quality of the solution of Poiseuille flow: error norm N_e at $Re = 100$.

β	5.0	6.0	7.0	8.0	9.0	10.0
N_e	1.59e−6	7.31e−7	3.16e−7	2.70e−7	4.18e−7	1.97e−7

Table II. Error norm N_e of the solution of Poiseuille flow at $\beta = 8.0$ for some Reynolds numbers.

Re	1.0e0	1.0e1	1.0e2	1.0e3	1.0e4	1.0e5
N_e	2.75e−7	2.73e−7	2.70e−7	1.06e−6	1.09e−5	1.10e−4

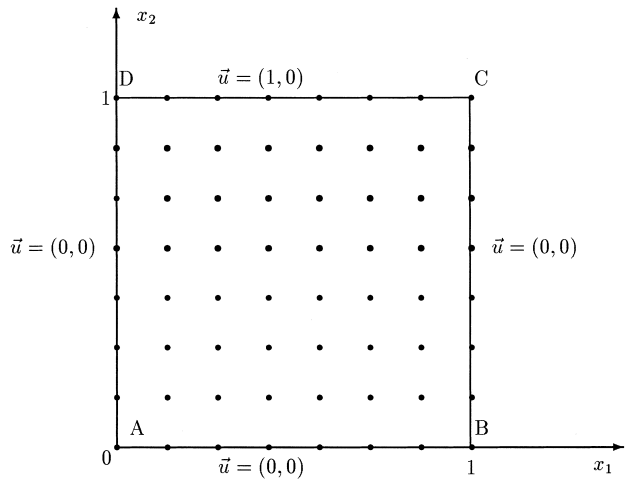

Figure 3. Driven cavity flow: note that the centre distribution is schematic only.

$$\psi = 0, \quad \psi_{,2} = 0 \quad \text{on the line } x_2 = 0 \tag{21}$$

$$\psi = 0, \quad \psi_{,1} = 0 \quad \text{on the line } x_1 = 1 \tag{22}$$

$$\psi = 0, \quad \psi_{,2} = 1 \quad \text{on the line } x_2 = 1 \tag{23}$$

$$\psi = 0, \quad \psi_{,1} = 0 \quad \text{on the line } x_1 = 0 \tag{24}$$

It is observed that adding some extra boundary conditions on the vorticity ω at the corners of the cavity makes the solution more accurate. The extra boundary conditions used here are $\omega_A = 0$, $\omega_B = 0$ (lower corners) and $\omega_C = \omega_D$ (upper corners) (Figure 3). Three uniform centre densities, namely 11×11, 17×17 and 21×21, are employed in the simulation for $Re = 100$ and the results are in good agreement with the benchmark solutions provided by Ghia *et al.* [22] (where a density of 129×129 was used) as shown in Tables III, IV and V and Figures 4 and 5. Table VI shows the total CPU times used to obtain a converged solution. Furthermore, the present IRBFN results are compared with FVM, FEM and BDIM results on the same density of 21×21 showing that the accuracy of the present method is very comparable with the accuracy of the BDIM method of Ramsak and Skerget [23], which is far more accurate than the FEM and FVM results (Table VII). The FVM and FEM results mentioned here are extracted from the paper by Ramsak and Skerget [23], where the FVM results were produced by the commercial code *TASCflow* (by Advanced Scientific Computing) and the FEM results by the commercial code *FIDAP* (by Fluid Dynamics International). At higher Reynolds number, a higher density of centres needs to be employed. Figures 6 and 7 show that IRBFN results for $Re = 400$ using the uniform density of 33×33 are very close to the benchmark solution of Ghia *et al.* [22] using a density of 129×129. In conclusion, the present method achieves very good solution with relatively low collocation densities.

Table III. Driven cavity flow, $Re = 100$: comparison of the minimum (algebraic) value of the velocity component u_1 on the vertical centreline with the benchmark solution (Bench.) obtained by Ghia *et al.* [22][a].

β	$(u_1)_{\min}$			
	IRBFN 11×11	IRBFN 17×17	IRBFN 21×21	Bench. [22] 129×129
3.1	-0.220	-0.215	-0.216	-0.211
3.3	-0.219	-0.216	-0.216	-0.211
3.5	-0.218	-0.216	-0.215	-0.211
3.7	-0.218	-0.215	-0.215	-0.211
3.9	-0.214	-0.213	-0.214	-0.211
4.1	—	-0.240	-0.215	-0.211

[a] The combined effect of β and centre densities is illustrated. The range of acceptable values of β is wider for higher centre densities.

Table IV. Driven cavity flow, $Re = 100$: comparison of the minimum (algebraic) value of the velocity component u_2 on the horizontal centreline with the benchmark solution (Bench.) obtained by Ghia *et al.* [22][a].

β	$(u_2)_{\min}$			
	IRBFN 11×11	IRBFN 17×17	IRBFN 21×21	Bench. [22] 129×129
3.1	-0.273	-0.257	-0.256	-0.245
3.3	-0.272	-0.260	-0.255	-0.245
3.5	-0.270	-0.257	-0.256	-0.245
3.7	-0.269	-0.257	-0.255	-0.245
3.9	-0.262	-0.258	-0.255	-0.245
4.1	—	-0.247	-0.254	-0.245

[a] The combined effect of β and centre densities is illustrated. The range of acceptable values of β is wider for higher centre densities.

3. NATURAL CONVECTION IN A SQUARE SLOT

The disadvantage of the driven cavity problem is that the moving lid introduces singularities at two of the corners. At the upper corners, the velocity is discontinuous and the vorticity is unbounded. A more realistic benchmark problem was devised by de Vahl Davis *et al.* [24] where the natural convection of a Boussinesq material in an enclosed cavity is induced by an imposed wall temperature difference. In this problem, the geometric simplicity of the driven cavity is maintained while the singularities are removed. Specifically, non-trivial motion is induced by maintaining the temperatures of the vertical walls constant but different between the two walls. The two horizontal walls are adiabatic and the direction of gravity is parallel to the vertical walls. Although the governing equations now include buoyancy terms, this problem is more realistic as it contains no singularities as in the case of the driven cavity problem (Roache [21]). The problem definition is shown in Figure 8.

Table V. Driven cavity flow, $Re = 100$: comparison of the maximum (algebraic) value of the velocity component u_2 on the horizontal centreline with the benchmark solution (Bench.) obtained by Ghia *et al.* [22][a].

β	$(u_2)_{\max}$			
	IRBFN 11×11	IRBFN 17×17	IRBFN 21×21	Bench. [22] 129×129
3.1	0.191	0.183	0.181	0.175
3.3	0.189	0.183	0.181	0.175
3.5	0.188	0.182	0.181	0.175
3.7	0.188	0.181	0.181	0.175
3.9	0.183	0.180	0.180	0.175
4.1	—	0.202	0.181	0.175

[a] The combined effect of β and centre densities is illustrated. The range of acceptable values of β is wider for higher centre densities.

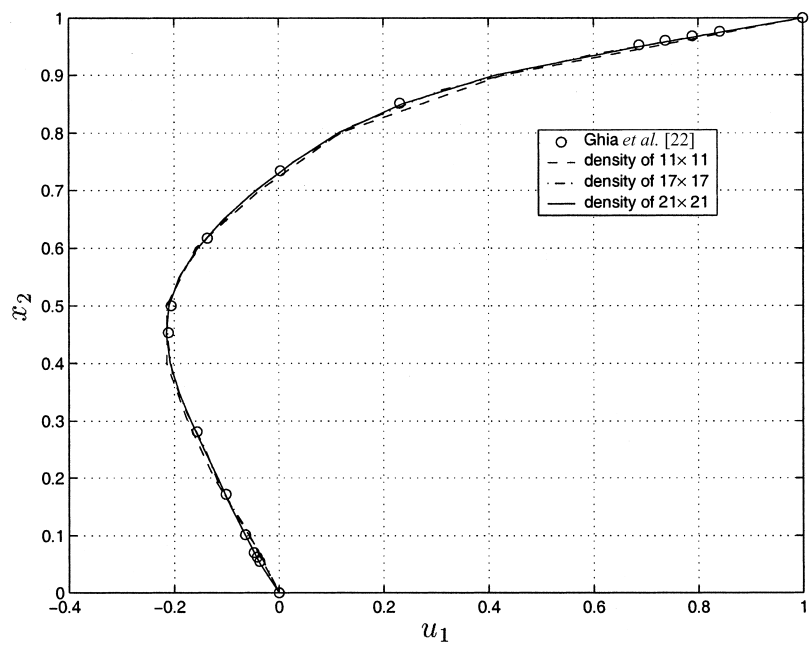

Figure 4. Driven cavity flow, $Re = 100$, $\beta = 3.9$: comparison of the x_1-component of the velocity profile on the vertical centreline with the benchmark solution obtained by Ghia *et al.* [22] (see legend Ghia *et al.* [22]).

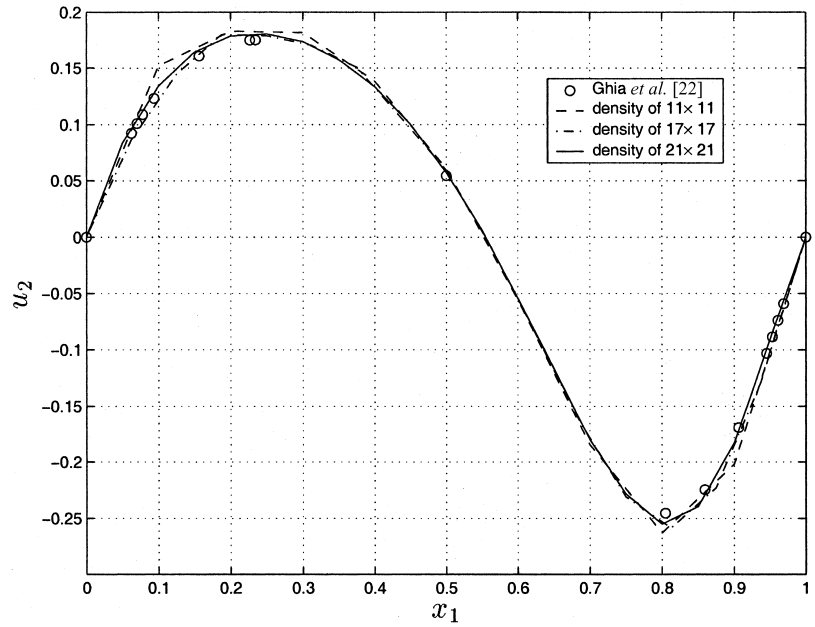

Figure 5. Driven cavity flow, $Re = 100$, $\beta = 3.9$: comparison of the x_1-component of the velocity profile on the horizontal centreline with the benchmark solution obtained by Ghia *et al.* [22] (see legend Ghia *et al.* [22]).

Table VI. Driven cavity flow, $Re = 100$: total CPU time used to obtain a converged solution[a].

Density	Matrix size	CPU time (s)
11×11	571×588	115
17×17	1291×1308	1182
21×21	1931×1948	3767

[a] The code is written in the MATLAB language (version 5.3R11 by The MathWorks, Inc.), which was run on a 233-MHz Pentium II PC. Note that MATLAB language is interpretative.

3.1. Governing equations

The equations governing the temperature and velocity behaviour can be cast in terms of vorticity–stream function variables and non-dimensionalized (using a similar scheme as in Leonard and Drummond [25]) by scaling the velocities by $U = \alpha g L^2 \Delta T / \nu$ where α is the coefficient of volumetric expansion, g the strength of the gravitational field and ΔT the temperature difference between the two vertical walls. The cavity dimensions are scaled by L and the temperatures are calculated with respect to the cold wall and scaled with ΔT. The

Table VII. Driven cavity flow, $Re = 100$: comparison of extreme velocity values computed at $\beta = 3.9$ with FEM, FVM and BDIM results using the centre density of 21×21, which is the same for all four methods[a].

Velocity	IRBFN	FEM [23]	FVM [23]	BDIM [23]	Bench. [22] (density 129×129)
$(u_1)_{\min}$	-0.214	-0.178	-0.191	-0.213	-0.211
Error (%)	1.42	15.64	9.48	0.95	
$(u_2)_{\min}$	-0.255	-0.217	-0.233	-0.259	-0.245
Error (%)	4.08	11.43	4.90	5.71	
$(u_2)_{\max}$	$+0.180$	$+0.152$	$+0.160$	$+0.177$	$+0.175$
Error (%)	2.86	13.14	8.57	1.14	

[a] The FEM results were obtained by Ramsak and Skerget [23] using *FIDAP* and the FVM results were also obtained by Ramsak and Skerget [23] using *TASCflow*.

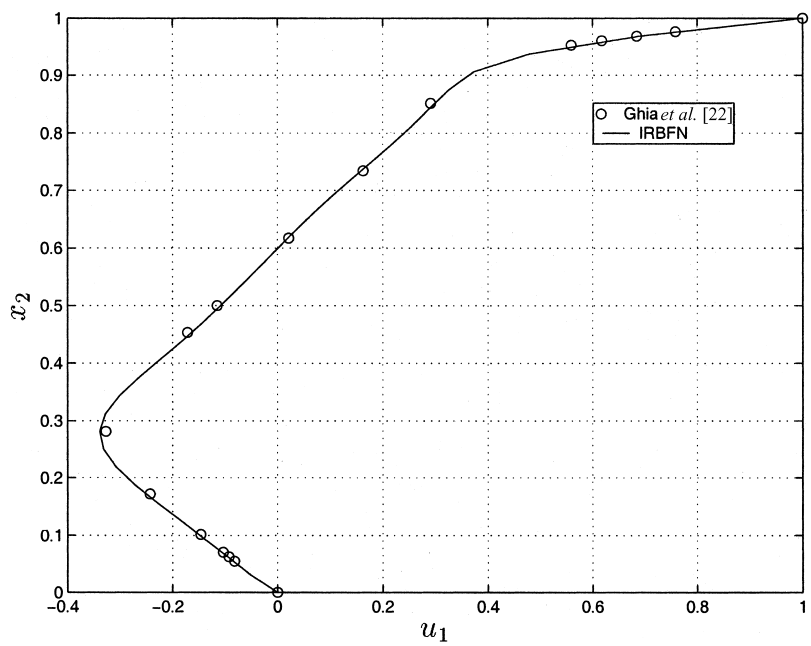

Figure 6. Driven cavity flow, $Re = 400$, $\beta = 2.9$: comparison of the x_1-component of the velocity profile on the vertical centreline using the centre density of 33×33 with the benchmark solution obtained by Ghia *et al.* [22] (see legend Ghia *et al.* [22]).

vorticity ω and streamfunction ψ are scaled with U/L and UL respectively. Applying the standard Boussinesq approximation yields the following forms of the Poisson, vorticity transport and energy equations:

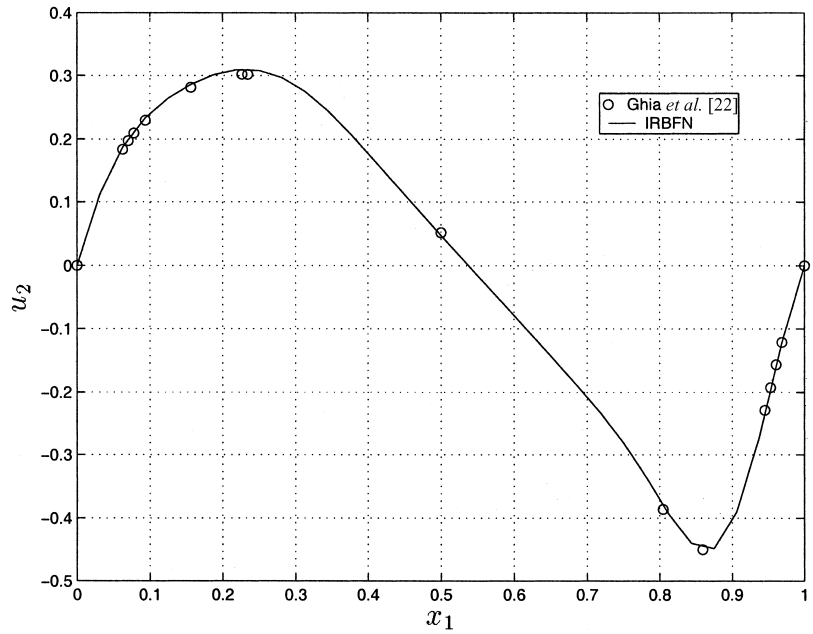

Figure 7. Driven cavity flow, $Re = 400$, $\beta = 2.9$: comparison of the x_1-component of the velocity profile on the horizontal centreline using the centre density of 33×33 with the benchmark solution obtained by Ghia *et al.* [22] (see legend Ghia *et al.* [22]).

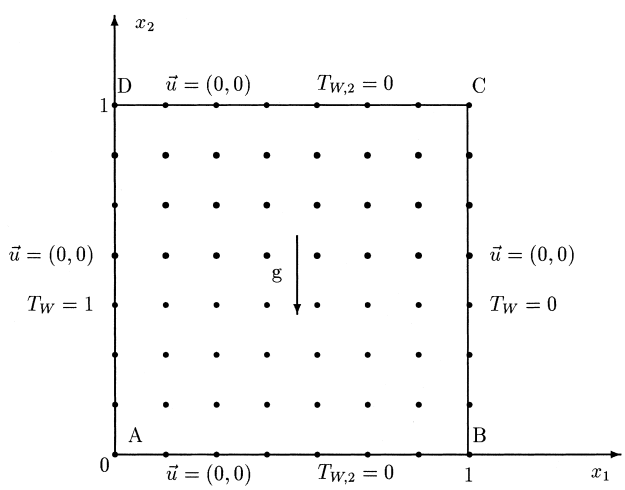

Figure 8. Natural convection flow in a square slot: note that the centre distribution is schematic only.

$$\omega + (\psi_{,11} + \psi_{,22}) = 0, \quad \mathbf{x} \in \Omega \tag{25}$$

$$(\omega_{,11} + \omega_{,22}) + T_{,1} = Gr(\psi_{,2}\omega_{,1} - \psi_{,1}\omega_{,2}), \quad \mathbf{x} \in \Omega \tag{26}$$

$$T_{,11} + T_{,22} = PrGr(\psi_{,2}T_{,1} - \psi_{,1}T_{,2}), \quad \mathbf{x} \in \Omega \tag{27}$$

where the Grashof number is defined as $Gr = UL/v$ while the Prandtl number is $Pr = v/\kappa$ where κ is the thermal diffusivity, $T_{,i} \equiv \partial T/\partial x_i$, $T_{,ij} \equiv \partial^2 T/\partial x_i\, \partial x_j$ and other symbols have been defined earlier. Note that the Rayleigh number $Ra = GrPr$.

The present scheme of non-dimensionalization results in the dimensionless velocity that is related to the one produced by the scheme used in the benchmark solution (de Vahl Davis [26]) according to

$$Ra(u_{\text{present}}) = u_{\text{bench}}$$

The advantage of the present non-dimensionalization scheme is that material properties only appear on the right-hand sides of the governing equations, which are estimated iteratively as described in Section 3.3. Thus, the system matrix, which is formed based on the left hand sides of the governing equations, needs to be singular value decomposed only once for all values of Rayleigh number and also for all subsequent iterations, provided that the centre distribution, the collocation point distribution and β are fixed, which is the case here.

3.2. Boundary conditions

The boundary conditions are as follows:

$$\psi = 0, \quad \psi_{,2} = 0, \quad T_{,2} = T_{\mathrm{W},2} = 0 \quad \text{on the line } x_2 = 0 \tag{28}$$

$$\psi = 0, \quad \psi_{,1} = 0, \quad T = T_{\mathrm{W}} = 0 \quad \text{on the line } x_1 = 1 \tag{29}$$

$$\psi = 0, \quad \psi_{,2} = 0, \quad T_{,2} = T_{\mathrm{W},2} = 0 \quad \text{on the line } x_2 = 1 \tag{30}$$

$$\psi = 0, \quad \psi_{,1} = 0, \quad T = T_{\mathrm{W}} = 1 \quad \text{on the line } x_1 = 0 \tag{31}$$

3.3. Numerical formulation based on RBFNs

In a similar manner as explained in Section 2.3, the RBFNs for the present problem are designed based on the following SSE, derived from the governing equations (25)–(27) together with boundary conditions (28)–(31):

$$\mathrm{SSE} = \sum_{\boldsymbol{x}^{(i)} \in \Omega} [(\psi_{,11}(\boldsymbol{x}^{(i)}) + \psi_{,22}(\boldsymbol{x}^{(i)})) + \omega^1(\boldsymbol{x}^{(i)})]^2$$

$$+ \sum_{\boldsymbol{x}^{(i)} \in \Omega} \{(\omega_{,11}(\boldsymbol{x}^{(i)}) + \omega_{,22}(\boldsymbol{x}^{(i)})) + T_{,1}(\boldsymbol{x}^{(i)}) - Gr[\psi_{,2}(\boldsymbol{x}^{(i)})\omega_{,1}(\boldsymbol{x}^{(i)}) - \psi_{,1}(\boldsymbol{x}^{(i)})\omega_{,2}(\boldsymbol{x}^{(i)})]\}^2$$

Table VIII. Natural convection in a square slot, $Ra = 1.0e3$: effect of β on the IRBFN result using the centre density of 11×11[a].

β	4.5	5.0	5.5	6.0	6.5	7.0	Bench. [26]
$(u_1)_{\max}$	3.659	3.659	3.654	3.653	3.657	3.656	3.649
x_2	0.813	0.813	0.814	0.814	0.814	0.814	0.813
$(u_2)_{\max}$	3.707	3.706	3.700	3.699	3.704	3.706	3.697
x_1	0.178	0.178	0.178	0.178	0.178	0.178	0.178
$\underline{Nu}_0$	1.119	1.119	1.119	1.118	1.118	1.118	1.117
$\overline{Nu}$	1.118	1.118	1.118	1.118	1.118	1.118	1.118

[a] The benchmark solution (Bench.) by de Vahl Davis [26] is also shown.

$$+ \sum_{\boldsymbol{x}^{(i)} \in \Omega} \{(T_{,11}(\boldsymbol{x}^{(i)}) + T_{,22}(\boldsymbol{x}^{(i)})) - PrGr[\psi_{,2}(\boldsymbol{x}^{(i)})T_{,1}(\boldsymbol{x}^{(i)}) - \psi_{,1}(\boldsymbol{x}^{(i)})T_{,2}(\boldsymbol{x}^{(i)})]\}^2$$

$$+ \sum_{\boldsymbol{x}^{(i)} \in \Omega} \{[(\psi^1(\boldsymbol{x}^{(i)}) - \psi^2(\boldsymbol{x}^{(i)})]^2 + [\omega^1(\boldsymbol{x}^{(i)}) - \omega^2(\boldsymbol{x}^{(i)})]^2 + [T^1(\boldsymbol{x}^{(i)}) - T^2(\boldsymbol{x}^{(i)})]^2\}$$

$$+ \sum_{\boldsymbol{x}^{(i)} \in \Gamma} \{[(\psi(\boldsymbol{x}^{(i)})]^2 + [\psi_{,n}(\boldsymbol{x}^{(i)}) - v_{\mathrm{W}}(\boldsymbol{x}^{(i)})]^2\} + \sum_{\boldsymbol{x}^{(i)} \in \Gamma} [T(\boldsymbol{x}^{(i)}) - T_{\mathrm{W}}(\boldsymbol{x}^{(i)})]^2$$

$$+ \sum_{\boldsymbol{x}^{(i)} \in \Gamma} [T_{,n}(\boldsymbol{x}^{(i)}) - T_{\mathrm{W}}(\boldsymbol{x}^{(i)})]^2 \tag{32}$$

where $\Gamma = \Gamma_1 \cup \Gamma_2$, Γ_1 and Γ_2 are the Dirichlet and Neumann boundaries respectively for the temperature T. Typically T^i denotes the temperature T obtained symbolically via $T_{,ii}$ in the manner explained previously in Section 2.3. Here the non-linear terms $\psi_{,2}\omega_{,1}$, $\psi_{,1}\omega_{,2}$, $\psi_{,2}T_{,1}$, $\psi_{,1}T_{,2}$ are treated iteratively in the same way as described above in Section 2.3.

3.4. Numerical results

In the present problem the convergence criterion is set at $\mathrm{tol} = 1.0e-6$. Table VIII presents the comparison of the present results at $Ra = 1.0e3$ (the Prandtl number is 0.71) with the benchmark solution obtained by de Vahl Davis [26], for the following variables:

1. Maximum horizontal velocity $(u_1)_{\max}$ on the vertical mid-plane and its location;
2. Maximum vertical velocity $(u_2)_{\max}$ on the horizontal mid-plane and its location;
3. Average Nusselt number value on the vertical boundary of the cavity at $x_1 = 0$, which is defined by

$$Nu_0 = Nu_1|_{x_1 = 0}$$

where

$$Nu_1(x_1) = \int_0^1 (u_1 T - T_{,1})\, \mathrm{d}x_2 \tag{33}$$

4. The average Nusselt number throughout the cavity, which is defined by

$$\overline{Nu} = \int_0^1 Nu_1 \, \mathrm{d}x_1 \tag{34}$$

Integrals (33) and (34) are computed using Simpson's rule. The agreement can be seen to be very good for all values of $4.5 \leq \beta \leq 7$. With increasing Rayleigh number the shape of the solutions, e.g. T and ψ is more complicated with steep gradients. For the network to cope with these fast-varying functions, the width β has to be decreased while the density has to be increased. However, it is sufficient to demonstrate the good accuracy of the present method with the use of a less than optimum value of β. Thus, the following combinations are chosen to examine the quality of the solution as the Rayleigh number increases:

- Density 11×11 and $\beta = 4.5$ for Rayleigh numbers $1.0e3$, $1.0e4$ and $1.0e5$;
- Density 21×21 and $\beta = 3.5$ for Rayleigh numbers $1.0e3$, $1.0e4$, $1.0e5$ and $1.0e6$;
- Density 27×27 and $\beta = 3$ for Rayleigh numbers $1.0e6$;

The present results are compared with the FDM results of de Vahl Davis [26] and the benchmark solution (de Vahl Davis [26]) in Tables IX, X, XI and XII. The comparison shows that for the same nodal density the present IRBFN results are closer to the benchmark results, especially at higher Rayleigh numbers. This is particularly pleasing, as a conclusion may be that the present IRBFN method possesses a higher rate of 'h convergence'. Figures 9–11

Table IX. Natural convection in a square slot, $Ra = 1.0e3$: comparison between IRBFN and FDM results (de Vahl Davis [26]) using the same centre densities[a]

	IRBFN	FDM [26]	IRBFN	FDM [26]	Bench. [26]
Density	11×11		21×21		
β	4.5	—	3.5	—	—
$(u_1)_{\max}$	3.659	3.427	3.651	3.589	3.649
Error (%)	0.27	6.08	0.05	1.64	
x_2	0.813	0.801	0.813	0.811	0.813
Error (%)	0.00	1.48	0.00	0.25	
$(u_2)_{\max}$	3.707	3.449	3.699	3.629	3.697
Error (%)	0.27	6.71	0.05	1.84	
x_1	0.178	0.193	0.178	0.181	0.178
Error (%)	0.00	8.43	0.00	1.69	
Nu_0	1.119	1.105	1.118	1.113	1.117
Error (%)	0.18	1.07	0.09	0.36	
$\overline{Nu}$	1.118	1.096	1.118	1.111	1.118
Error (%)	0.00	1.97	0.00	0.63	

[a] The benchmark solution (Bench.) by de Vahl Davis [26] is also shown.

Table X. Natural convection in a square slot, $Ra = 1.0e4$: comparison between IRBFN and FDM results (de Vahl Davis [26]) using the same centre densities[a].

	IRBFN	FDM [26]	IRBFN	FDM [26]	Bench. [26]
Density	11×11		21×21		
β	4.5	—	3.5	—	—
$(u_1)_{\max}$	16.206	16.243	16.195	16.189	16.178
Error (%)	0.17	0.40	0.11	0.07	
x_2	0.824	0.808	0.823	0.820	0.823
Error (%)	0.12	1.82	0.00	0.36	
$(u_2)_{\max}$	19.639	18.005	19.642	19.197	19.617
Error (%)	0.11	8.22	0.13	2.14	
x_1	0.119	0.139	0.119	0.125	0.119
Error (%)	0.00	16.81	0.00	5.04	
Nu_0	2.271	2.307	2.248	2.255	2.238
Error (%)	1.47	3.08	0.45	0.76	
$\overline{Nu}$	2.244	2.171	2.246	2.212	2.243
Error (%)	0.04	3.21	0.13	1.38	

[a] The benchmark solution (Bench.) by de Vahl Davis [26] is also shown.

Table XI. Natural convection in a square slot, $Ra = 1.0e5$: comparison between IRBFN and FDM results (de Vahl Davis [26]) using the same centre densities[a].

	IRBFN	FDM [26]	IRBFN	FDM [26]	Bench. [26]
Density	11×11		21×21		
β	4.5	—	3.5	—	—
$(u_1)_{\max}$	33.961	40.90	34.790	36.46	34.73
Error (%)	2.21	17.77	0.17	4.98	
x_2	0.850	0.846	0.855	0.854	0.855
Error (%)	0.58	1.05	0.00	0.12	
$(u_2)_{\max}$	67.533	59.71	68.694	62.79	68.59
Error (%)	1.54	12.95	0.15	8.46	
x_1	0.067	0.083	0.066	0.075	0.066
Error (%)	1.52	25.76	0.00	13.64	
Nu_0	4.773	4.767	4.583	4.716	4.509
Error (%)	5.85	5.72	1.64	4.59	
$\overline{Nu}$	4.488	4.446	4.525	4.454	4.519
Error (%)	0.69	1.62	0.13	1.44	

[a] The benchmark solution (Bench.) by de Vahl Davis [26] is also shown.

display the corresponding distribution of temperature, velocity vectors and vorticity obtained by the present IRBFN method for the Rayleigh number $Ra = 1.0e6$. The plots are in good agreement with the benchmark results.

Table XII. Natural convection in a square slot, $Ra = 1.0e6$: comparison between IRBFN and FDM results (de Vahl Davis [26]) using the centre density of 21×21[a].

	IRBFN	FDM [26]	IRBFN	Bench. [26]
Density	21×21		27×27	
β	3.5	—	3.0	—
$(u_1)_{\max}$	64.31	79.27	64.65	64.63
Error (%)	0.50	22.65	0.03	
x_2	0.851	0.862	0.850	0.850
Error (%)	0.12	1.41	0.00	
$(u_2)_{\max}$	218.93	195.44	220.29	219.36
Error (%)	0.20	10.90	0.42	
x_1	0.037	0.045	0.037	0.038
Error (%)	2.63	18.42	2.63	
Nu_0	9.442	9.502	9.273	8.817
Error (%)	7.09	7.77	5.17	
$\overline{Nu}$	8.694	9.027	8.798	8.800
Error (%)	1.20	2.58	0.02	

[a] The IRBFN result of the density 27×27 and the benchmark solution (Bench.) by de Vahl Davis [26] are also shown.

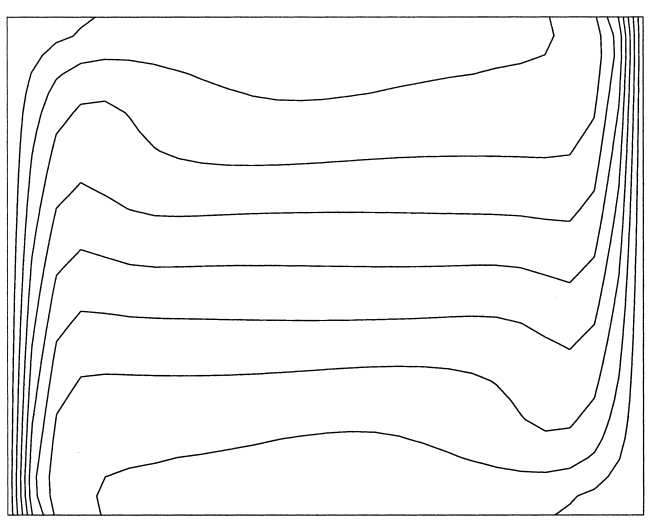

Figure 9. Natural convection in a square slot, $Ra = 1.0e6$, $\beta = 3.0$: temperature held obtained using the centre density of 27×27.

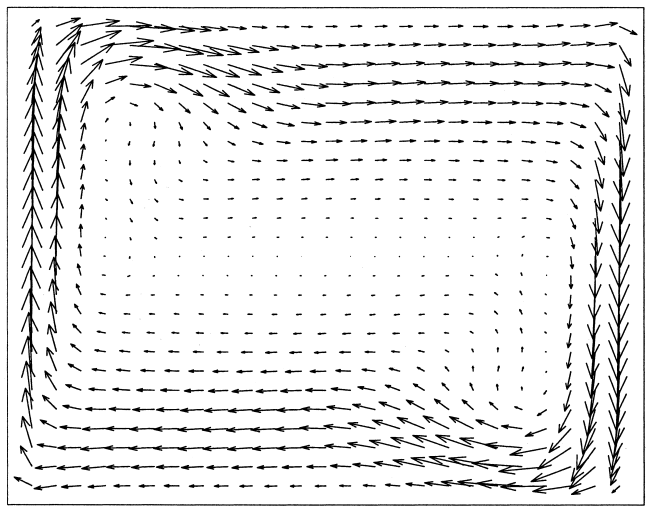

Figure 10. Natural convection in a square slot, $Ra = 1.0e6$, $\beta = 3.0$: velocity vector field obtained using the centre density of 27×27.

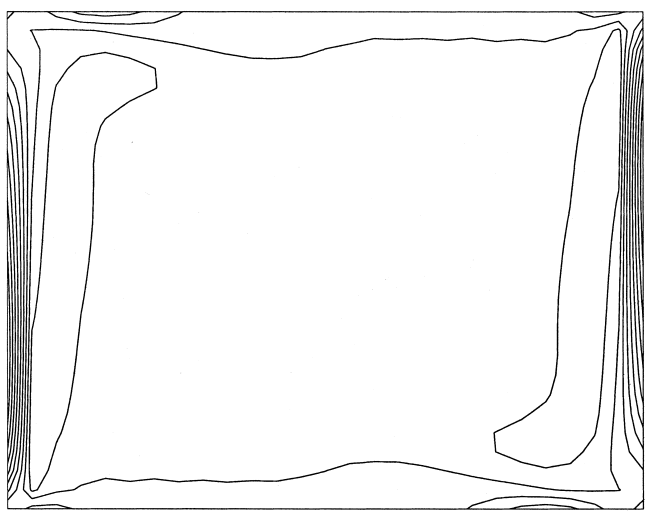

Figure 11. Natural convection in a square slot, $Ra = 1.0e6$, $\beta = 3.0$: vorticity field obtained using the centre density of 27×27.

4. CONCLUDING REMARKS

A new mesh-free numerical method for Navier–Stokes equations based on the concept of an IRBFN is developed, implemented and verified with a series of test problems. It is exciting that the method produces a good quality solution using only relatively low collocation densities and requires a minimal amount of effort to implement. In general, the most difficult step in using the RBFN-based methods is how to choose the optimum value of RBF widths. It is shown here that the present IRBFN method works very well with a very simple means of determining the RBF width according to the relation $a^{(i)} = \beta d^{(i)}$, where $d^{(i)}$ is simply the distance from the centre ith to its nearest neighbour and a single β value reasonably chosen as shown in example problems. Although the present IRBFN method is quite tolerant of the variation of β about a mean value in a given problem, a universal method of determining the RBF width for an arbitrary problem is still elusive. Fortunately, our cumulative experience so far indicates that β is in the range $1 \leq \beta \leq 10$, which is not too wide. A disadvantage of the present method is that the system matrix is dense. However, it is feasible that this disadvantage can be overcome by domain decomposition and parallelization which are topics currently under investigation.

ACKNOWLEDGMENTS

This work is supported by a Special USQ Research Grant (grant no. 179-310) to Thanh Tran-Cong. Nam Mai-Duy is supported by a USQ scholarship. This support is gratefully acknowledged.

REFERENCES

1. Roache PJ. *Fundamentals of Computational Fluid Dynamics* (2nd edn). Hermosa Publishers: Albuquerque, NM, 1998.
2. Smith GD. *Numerical Solution of Partial Differential Equations: Finite Difference Methods*. Clarendon Press: Oxford, 1978.
3. Cook RD, Malkus DS, Plesha ME. *Concepts and Applications of Finite Element Analysis*. Wiley: Toronto, 1989.
4. Fletcher CAJ. *Computational Galerkin Methods*. Springer: New York, 1984.
5. Hughes TJR. *The Finite Element Method*. Prentice-Hall: New Jersey, 1987.
6. Reddy JN, Gartling DK. *The Finite Element Method in Heat Transfer and Fluid Dynamics*. CRC Press: Boca Raton, FL, 1987.
7. Zienkiewicz OC, Taylor RL. *The Finite Element Method* (4th edn). McGraw-Hill: London, 1991.
8. Patankar SV. *Numerical Heat Transfer and Fluid Flow*. McGraw-Hill: New York, 1980.
9. Powell MJD. In radial basis functions for multivariable interpolation: a review. In *IMA Conference on Algorithms for the Approximation of Function and Data*, Watson JC, Cox MG (eds). Royal Military College of Science: Shrivenham, U.K., 1985; 143–167.
10. Broomhead DS, Lowe D. Multivariable functional interpolation and adaptive networks. *Complex Systems* 1988; **2**: 321–355.
11. Poggio T, Girosi F. Networks for approximation and learning. *Proceedings of the IEEE* 1990; **78**: 1481–1497.
12. Haykin S. *Neural Networks: A Comprehensive Foundation*. Prentice-Hall: New Jersey, 1999.
13. Kansa EJ. Multiquadrics—a scattered data approximation scheme with applications to computational fluid dynamics—I. Surface approximations and partial derivative estimates. *Computers and Mathematics with Applications* 1990; **19**(8/9): 127–145.
14. Moridis GJ, Kansa EJ. The Laplace transform multiquadrics method: a highly accurate scheme for the numerical solution of linear partial differential equations. *Journal of Applied Science and Computation* 1994; **1**(2): 375–407.
15. Kansa EJ. Multiquadrics—a scattered data approximation scheme with applications to computational fluid dynamics—II. Solutions to parabolic, hyperbolic and elliptic partial differential equations. *Computers and Mathematics with Applications* 1990; **19**(8/9): 147–161.

16. Dubal MR. Domain decomposition and local refinement for multiquadric approximations. I: second-order equations in one-dimension. *Journal of Applied Science and Computation* 1994; **1**(1): 146–171.
17. Sharan M, Kansa EJ, Gupta S. Application of the multiquadric method for numerical solution of elliptic partial differential equations. *Journal of Applied Science and Computation* 1997; **84**: 275–302.
18. Mai-Duy N, Tran-Cong T. Numerical solution of differential equations using multiquadric radial basis function networks. *Neural Networks* 2001; **14**: 185–199.
19. Mai-Duy N, Tran-Cong T. Approximation of function and its derivatives using radial basis function networks. *Neural Networks* (submitted).
20. Moody J, Darken CJ. Fast learning in networks of locally-tuned processing units. *Neural Computation* 1989; **1**: 281–294.
21. Roache PJ. *Verification and Validation in Computational Science and Engineering*. Hermosa Publishers: Albuquerque, NM, 1998.
22. Ghia U, Ghia KN, Shin CT. High-Re solutions for incompressible flow using the Navier–Stokes equations and a multigrid method. *Journal of Computational Physics* 1982; **48**: 387–411.
23. Ramsak M, Skerget L. Mixed boundary elements for laminar flows. *International Journal for Numerical Methods in Fluids* 1999; **31**: 861–877.
24. de Vahl Davis G, Jones IP, Roache PJ. Natural convection in an enclosed cavity: a comparison problem. *Computers and Fluids* 1979; **7**: 315–316.
25. Leonard BP, Drummond JE. Why you should not use 'Hybrid', 'Power law' or related exponential schemes for convective modelling—there are much better alternatives. *International Journal for Numerical Methods in Fluids* 1995; **20**: 421–442.
26. de Vahl Davis G. Natural convection of air in a square cavity: a bench mark numerical solution. *International Journal for Numerical Methods in Fluids* 1983; **3**: 249–264.

